Electronic effects due to organic linker-metal surface interactions: implications on screening of MOF-encapsulated catalysts

Benjamin Schweitzer,[a] ‡ Chloe Archuleta,[a] ‡ Bomsaerah Seong,[a] Ryther Anderson,[a] Diego A. Gómez-Gualdrón[a] *

[a] Department of Chemical and Biological Engineering, Colorado School of Mines, Golden CO 80401, USA

*Corresponding author: dgomezgualdron@mines.edu
‡ These authors contributed equally

Table of contents

Section S1. Additional Simulation Data
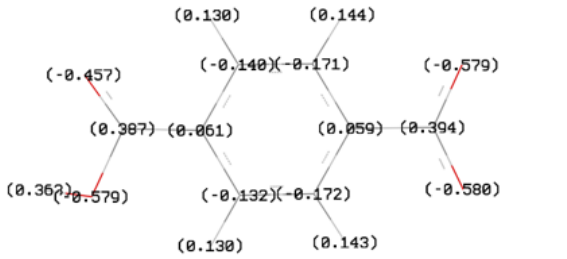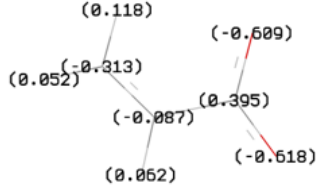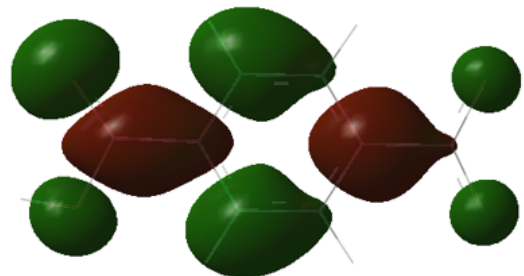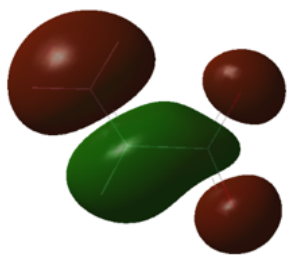
	Benzene dicarboxylate	Acrylate
charge distribution	(0.130) (0.144) (-0.457) (-0.140)(-0.171) (-0.579) (0.387) (0.061) (0.059) (0.394) (0.362)(-0.579) (-0.132)(-0.172) (-0.580) (0.130) (0.143)	(0.118) (-0.609) (0.052)(-0.313) (0.395) (-0.087) (-0.618) (0.062)
LUMO		

Figure S1. Comparison of electronic properties of benzene dicarboxylate (BDC), a common MOF linker, and acrylate, which is used to approximate the carboxylate moiety of BDC. Notice that *(i)* charges on the carboxylate moiety are similar in BDC and acrylate, and *(ii)* the shape of the LUMO on the α-C and carboxylate group are similar in BDC and acrylate.

Table S1. d-band center (eV) for reference surfaces

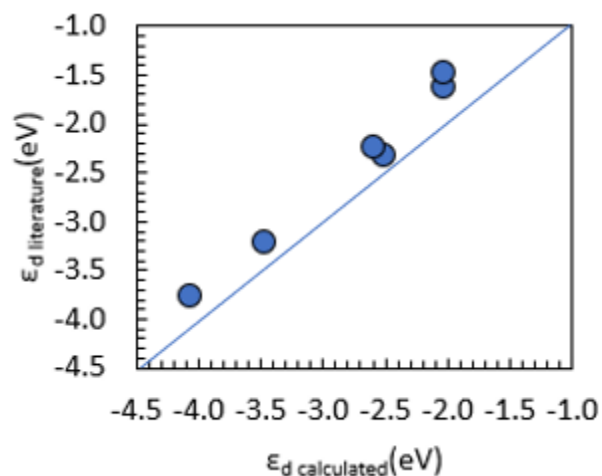| Metal	Linker-free slab	H-added Linker-free slab
Zn	-6.93	-
Ag	-3.76	-
Au	-3.21	-3.34
Cu	-2.33	-2.34
Pt	-2.24	-2.25
Pd	-1.62	-1.59
Ni	-1.47	-1.47

Figure S2. Parity plot comparing d-band center calculated by us (horizontal axis) on bare (i.e. linker-free) metal surfaces and those reported by Goddard and coworkers[1] (vertical axis).
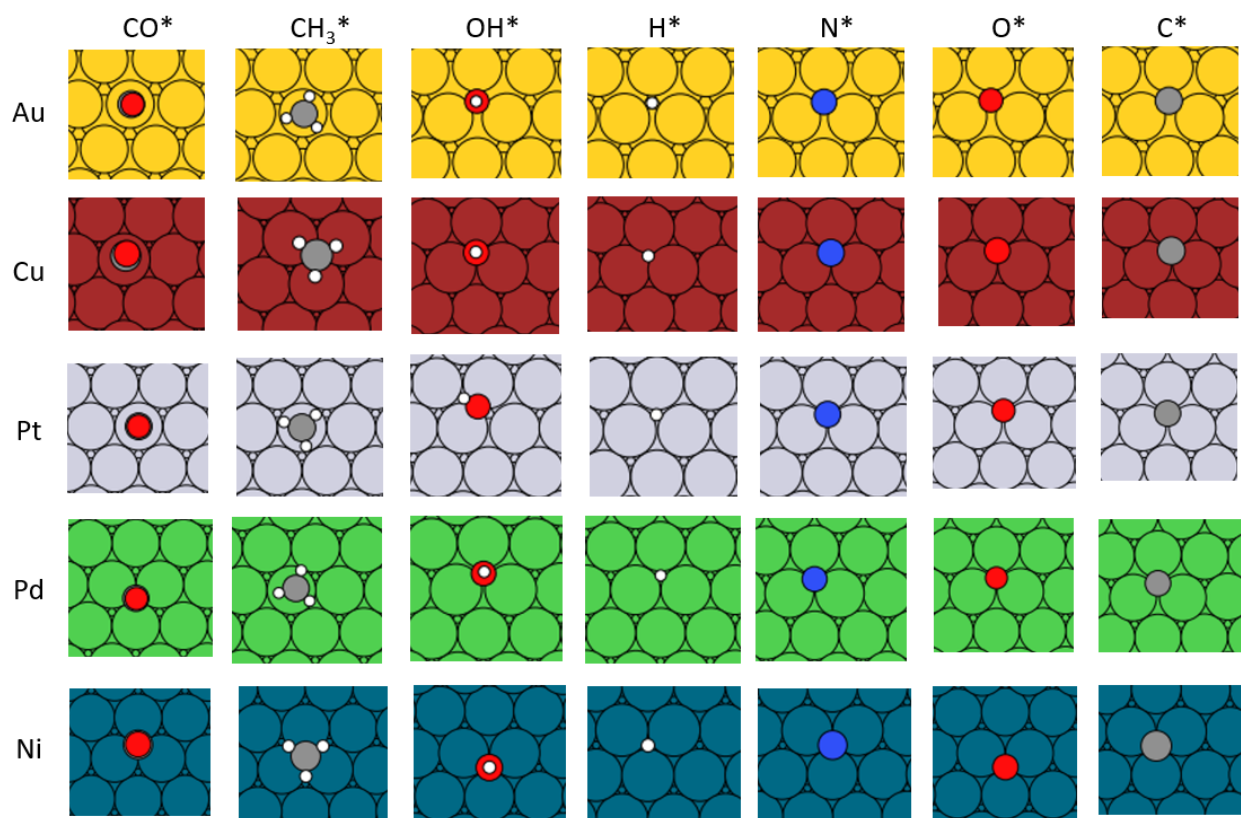

Figure S3. Optimized binding configurations of small adsorbates on bare surfaces.

Table S2. Binding energies E_{ads} (kJ/mol) of chemisorbed species on linker-free surfaces. Adsorption site is indicated as superscript. t = top site, f = fcc hollow site, h = hcp hollow site, b = bridge site.

Species	bare surface					H-added surface				
	Au	Cu	Pt	Pd	Ni	Au	Cu	Pt	Pd	Ni
CO*	-43 (t)	-101 (t)	-205 (t)	-221 (f)	-205 (f)	-46 (t)	-108 (t)	-208 (t)	-226 (f)	-210 (f)
CH₃*	-156 (t)	-179 (f)	-264 (t)	-212 (t)	-214 (f)	-163 (t)	-178 (f)	-266 (t)	-211 (t)	-217 (f)
H*	-209 (f)	-254 (f)	-273 (f)	-279 (f)	-273 (f)	-208 (f)	-256 (f)	-279 (f)	-283 (f)	-275 (f)
N*	-254 (f)	-396 (f)	-486 (f)	-478 (f)	-519 (f)	-253 (f)	-386 (f)	-492 (f)	-480 (f)	-529 (f)
OH*	-190 (f)	-320 (f)	-219 (b)	-260 (f)	-320 (f)	-193 (f)	-317 (f)	-216 (b)	-263 (f)	-325 (f)
O*	-313 (f)	-480 (f)	-425 (f)	-430 (f)	-515 (f)	-304 (f)	-470 (f)	-425 (f)	-435 (f)	-521 (f)
C*	-451 (f)	-519 (f)	-707 (f)	-697 (f)	-664 (f)	-455 (f)	-514 (f)	-710 (f)	-701 (f)	-667 (f)

Scaling relationships

$(E_{ads})_{C^{\bullet}} = -135\varepsilon_d - 901$ $(E_{ads})_{O^{\bullet}} = -64\varepsilon_d - 579$

$(E_{ads})_{CH3^{\bullet}} = -39\varepsilon_d - 287$ $(E_{ads})_{OH^{\bullet}} = -19\varepsilon_d - 312$

$(E_{ads})_{CO^{\bullet}} = -84\varepsilon_d - 342$ $(E_{ads})_{H^{\bullet}} = -28\varepsilon_d - 321$

$(E_{ads})_{N^{\bullet}} = -127\varepsilon_d - 707$

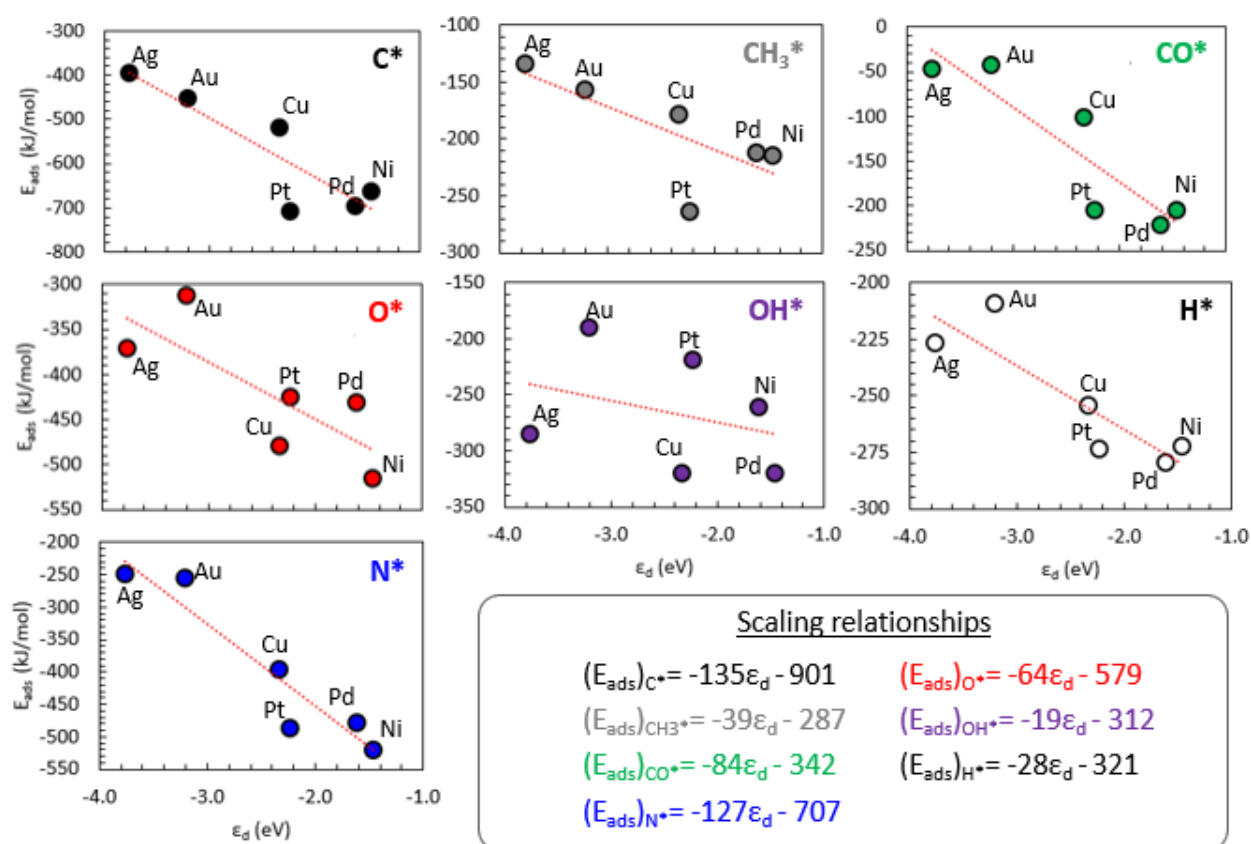**Figure S4.** Scaling relationships between binding energies (E_{ads}) and d-band centers for bare (i.e. linker-free) metal surfaces.

$(E_{ads})_{O^•} = -80\varepsilon_d - 575$

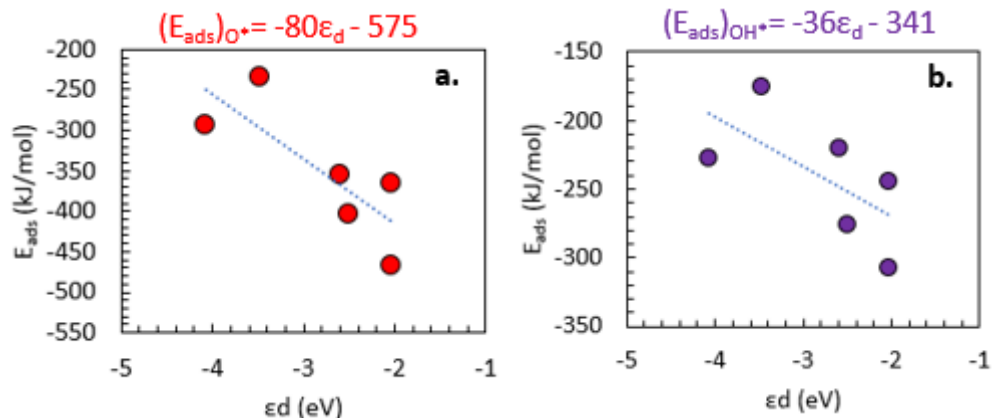$(E_{ads})_{OH^•} = -36\varepsilon_d - 341$

Figure S5. Scaling relationships plotted using the binding energy and d-band center data reported by Goddard and coworkers.[1] These plots and scaling relationships provide a comparison of our calculated values with those reported in the literature.

$(E_{ads})_{CH3^•} = 0.32(E_{ads})_{C^•} - 0.08$

$(E_{ads})_{OH^•} = 0.57(E_{ads})_{O^•} - 0.25$
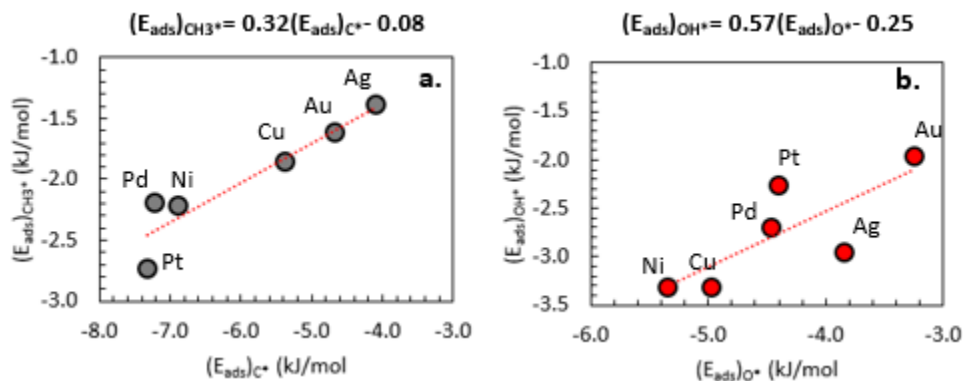
Figure S6. Scaling relationships between a) CH_3^* and C^* and b) OH^* and O^* binding energies on bare (i.e. linker-free) metal surfaces. As reference, using the RPBE functional, Norskov and coworkers[2] reported a relationship between CH_3^* and C^* given by $\mathbf{(E_{ads})_{CH3^*} = 0.26(E_{ads})_{C^*} + 0.14}$, and between OH^* and O^* given by $\mathbf{(E_{ads})_{OH^*} = 0.50(E_{ads})_{O^*} - 0.23}$. These plots and scaling relationships provide a comparison of our calculated values with those reported in the literature

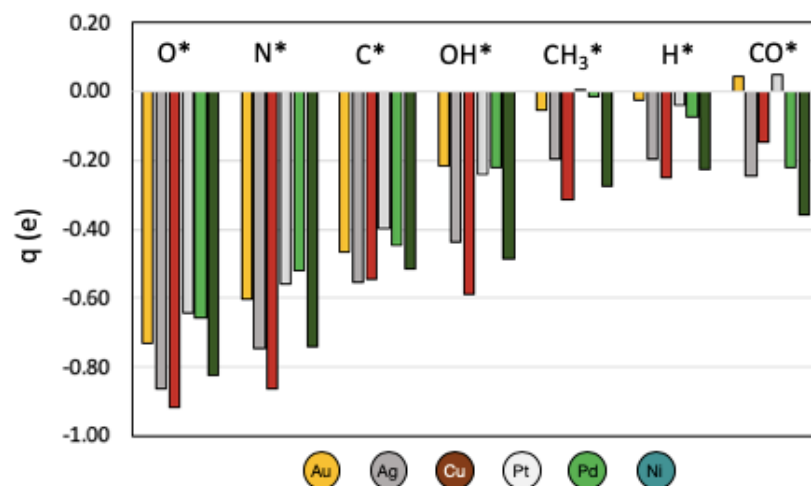**Figure S7.** Charge of adsorbates on different (111) metal surfaces. Each cluster of bars corresponds to one adsorbate. Color of bars indicate metal surfaces according to color code below the plot.
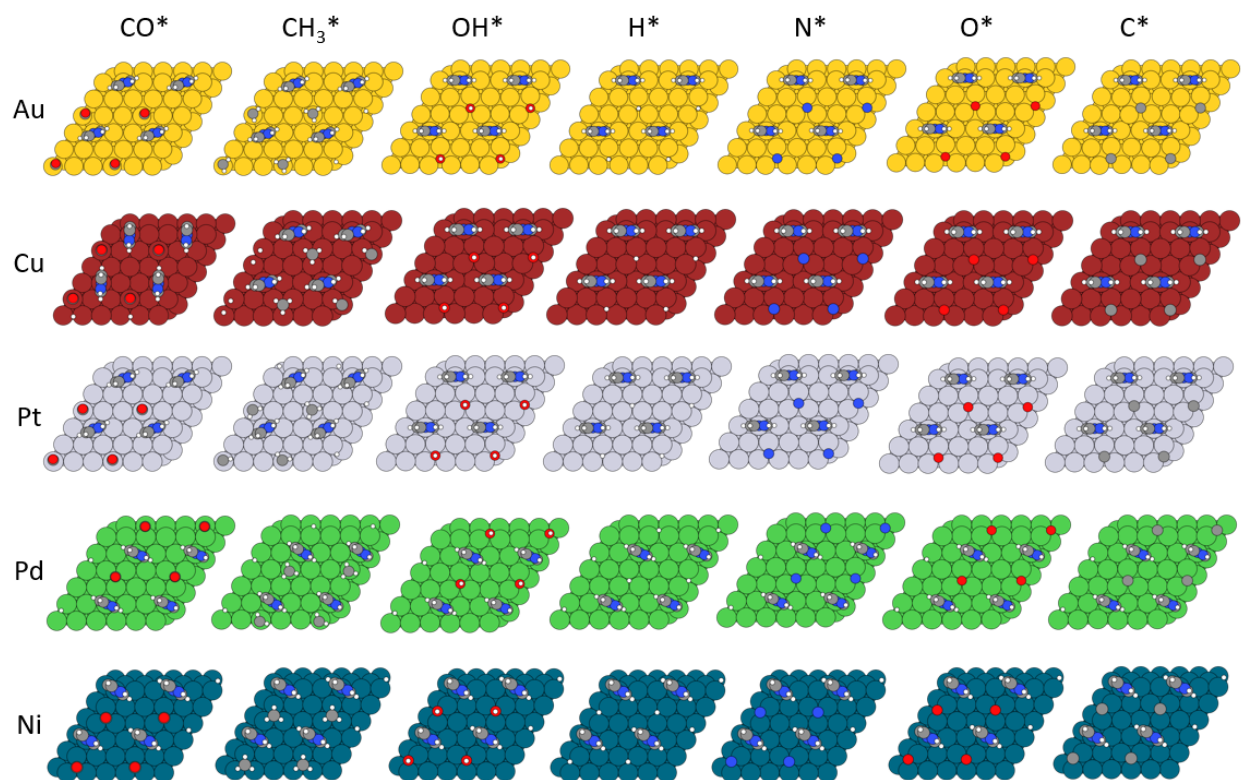
Figure S8. Optimized binding configurations of small adsorbates on surface with coordinated imidazole linker.

Table S3. Zero-point energy (ZPE) corrections and temperature effects on binding energies for test cases.

System	Frequencies (cm^{-1})	ZPE (kJ/mol)	ZPE effect on E_{ads} (kJ/mol)	TS$_{vib}$@300 K (kJ/mol)	TS$_{vib}$@423 K (kJ/mol)
CO binding					
Pt	2073, 487, 392, 392, 67, 65	20	8	14	26
Pt-I	2008, 488, 391, 375, 92, 62	20	8	14	25
Pt-C	2053, 488, 406, 392, 84, 62	20	8	14	25
Pt-T	2019, 494, 405, 385, 59, 52	20	8	15	27
H binding					
Pt	2089, 2065, 588	27	27	1	2
Pt-T	2081, 2060, 624	27	27	1	2
N binding					
Pt	642, 550, 588	10	10	2	5
Pt-T	640, 558, 555	10	10	2	5

Table S4. Binding energy differences of chemisorbed species between the linker-free and imidazolate-coordinated surface. $\Delta E_{ads} = (E_{ads})_{imidazole} - (E_{ads})_{bare}$ and $\%\Delta E_{ads} = [(E_{ads})_{imidazole} - (E_{ads})_{bare}]/(E_{ads})_{bare} \times 100$

Species	ΔE_{ads} (kJ/mol)					$\%\Delta E_{ads}$				
	Au	Cu	Pt	Pd	Ni	Au	Cu	Pt	Pd	Ni
CO*	-6	-14	2	-18	-29	-13	-14	1	-8	-14
CH₃*	1	3	4	2	4	0	2	1	1	2
H*	3	0	1	-3	-2	2	0	1	-1	-1
N*	-14	-10	10	0	-10	-6	-3	2	0	-2
OH*	6	15	30	11	13	3	5	14	4	4
O*	-10	-8	11	-2	-10	-3	-2	3	-1	-2
C*	-14	-8	15	0	-13	-3	-2	2	0	-2

Figure S9. Optimized binding configurations of small adsorbates on surface with coordinated carboxylate linker.

Table S5. Binding energy differences of chemisorbed species between the linker-free and carboxylate-coordinated surface. ΔE_{ads} = $(E_{ads})_{carboxylate}$ − $(E_{ads})_{bare}$ and $\%\Delta E_{ads} = [(E_{ads})_{carboxylate} − (E_{ads})_{bare}]/(E_{ads})_{bare}$ x 100

Species	ΔE_{ads} (kJ/mol)					$\%\Delta E_{ads}$				
	Au	**Cu**	**Pt**	**Pd**	**Ni**	Au	Cu	Pt	Pd	Ni
CO*	-16	-4	6	-6	-6	-34	-3	3	-3	-3
CH₃*	-4	-14	1	-7	-10	-2	-8	0	-3	-5
H*	8	2	5	-1	2	4	1	2	0	1
N*	10	3	15	5	5	4	1	3	1	1
OH*	4	0	-18	2	-3	2	0	2	1	-1
O*	4	4	10	6	-3	1	1	2	1	-1
C*	6	4	21	3	4	1	1	3	0	1

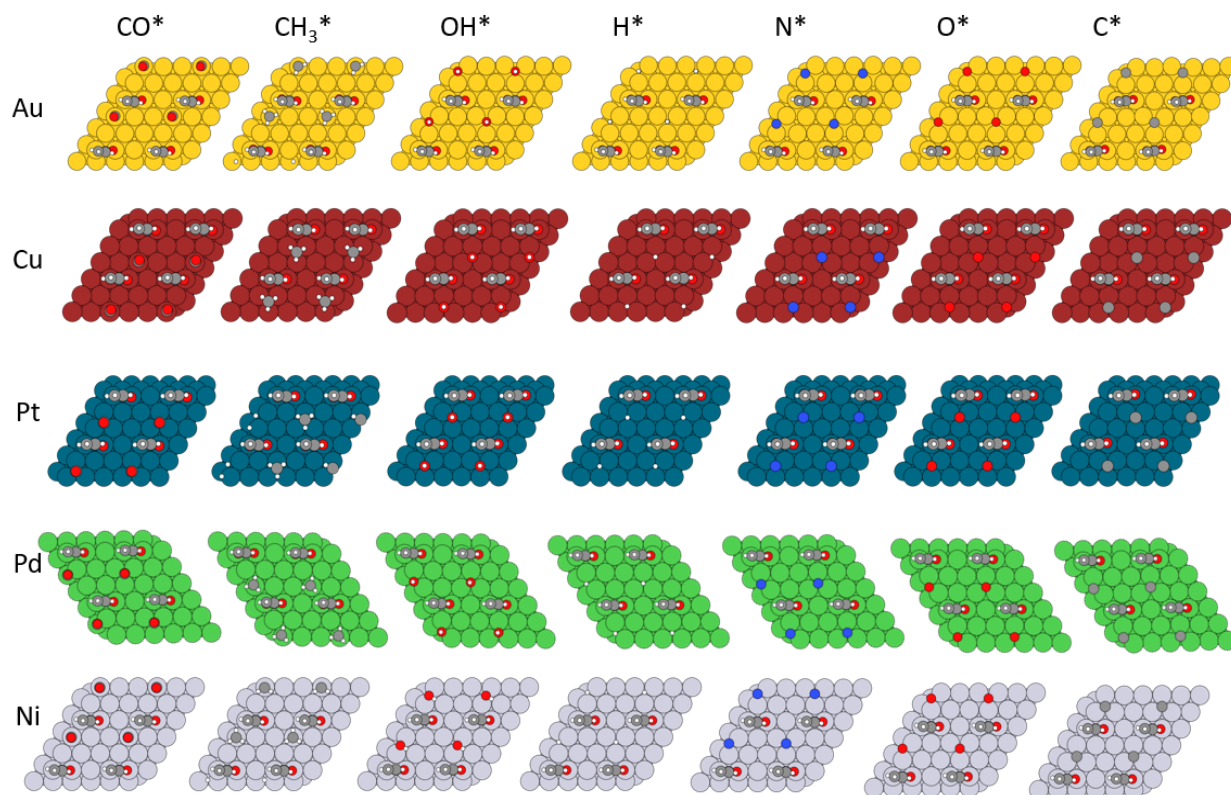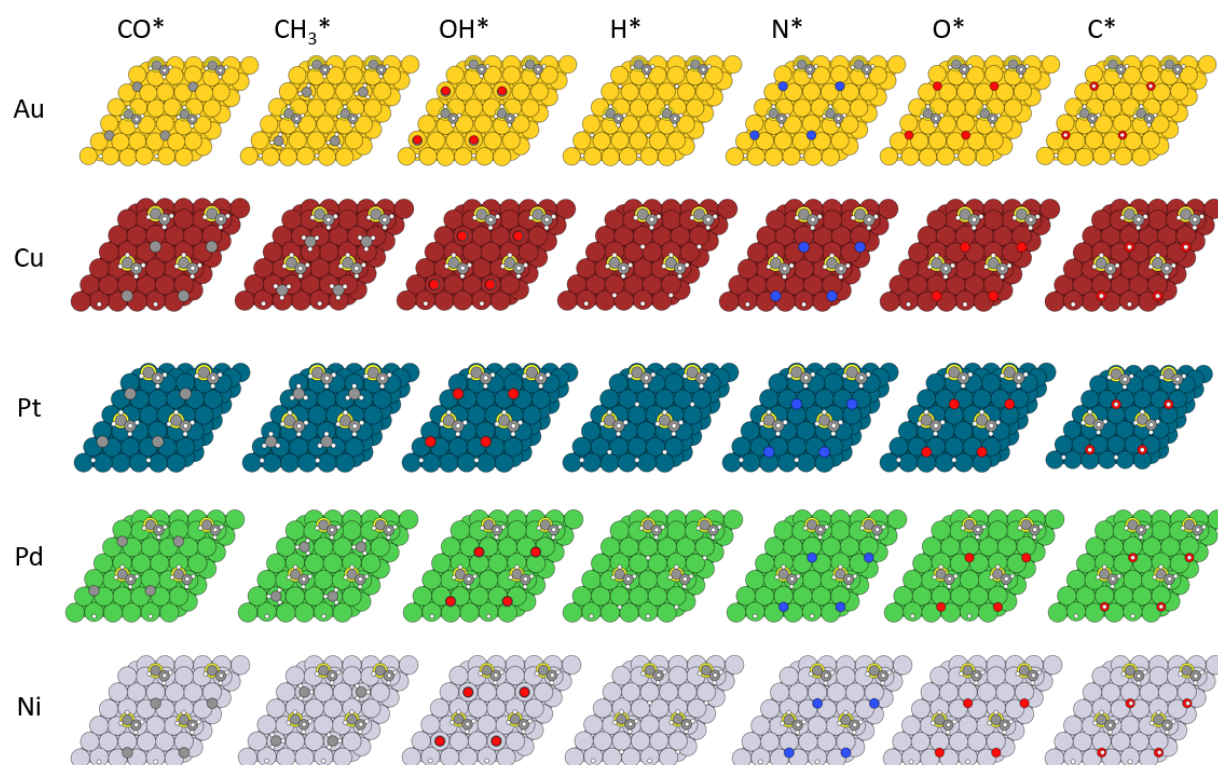**Figure S10**. Optimized binding configurations of small adsorbates on surface with coordinated carboxylate linker.

Table S6. Binding energy differences of chemisorbed species between the linker-free and thiolate-coordinated surface. $\Delta E_{ads} = (E_{ads})_{thiolate} - (E_{ads})_{bare}$ and $\%\Delta E_{ads} = [(E_{ads})_{thiolate} - (E_{ads})_{bare}]/(E_{ads})_{bare}$ x 100

| Species | ΔE_{ads} (kJ/mol) | | | | | $\%\Delta E_{ads}$ | | | | |
	Au	Cu	Pt	Pd	Ni	Au	Cu	Pt	Pd	Ni
CO*	-7	8	22	-8	-20	-13	7	11	-4	-9
CH₃*	10	-2	9	1	5	6	-1	3	0	2
H*	0	2	15	1	3	0	1	5	0	1
N*	-14	10	36	9	10	-6	3	7	2	2
OH*	2	17	38	18	16	2	5	17	7	5
O*	-16	3	32	14	2	-5	1	8	3	0
C*	-36	17	41	9	-5	-8	3	6	1	-1

Table S7. Changes in properties of surface bound CO due to presence of the linker (I = imidazole, C = carboxylate, T = thiolate).

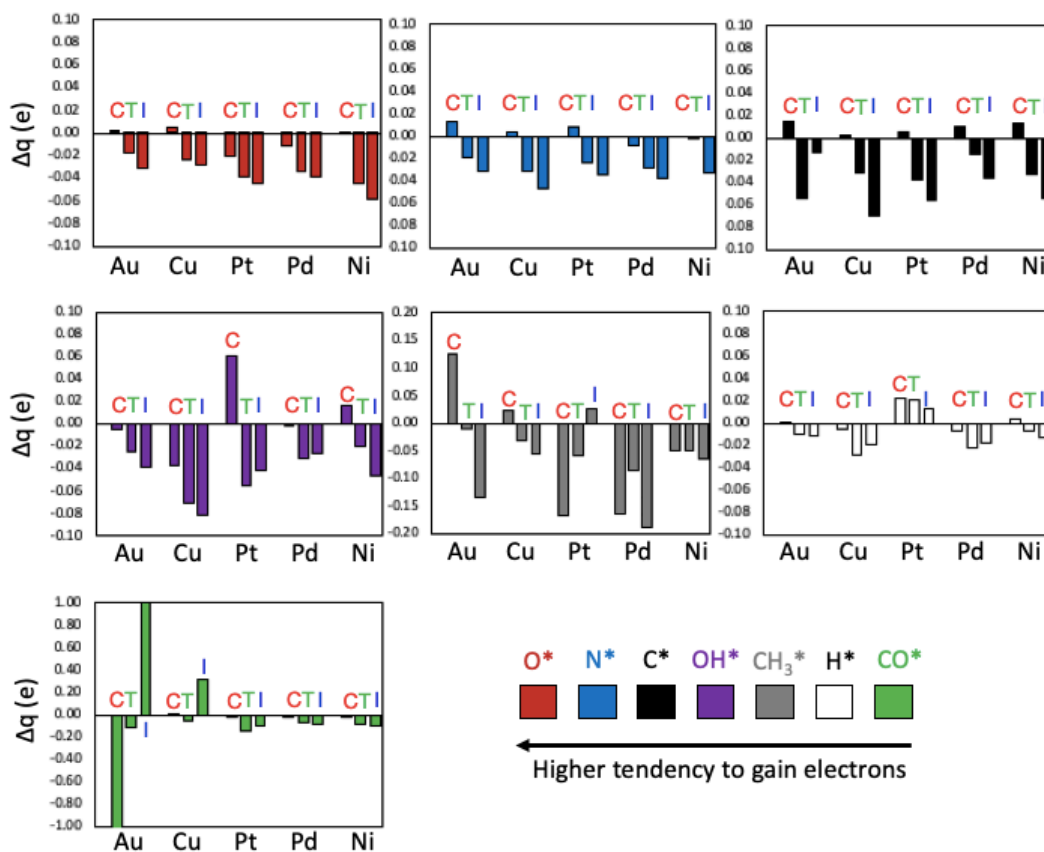| Metal	Linker	Δv (cm-1)	Δd_{C-O} (Å)	Δq (e)	ΔE_{ads}
Au	I	-56	0.007	-0.09	-6
Cu	I	-89	0.014	-0.13	-14
Pt	I	-65	0.009	-0.10	**2**
Pd	I	-49	0.008	-0.08	-18
Ni	I	-76	0.014	-0.09	-29
Au	T	-44	0.005	-0.11	-9
Cu	T	-44	0.006	-0.05	**1**
Pt	T	-53	0.008	-0.14	**19**
Pd	T	-37	0.006	-0.06	-13
Ni	T	-58	0.010	-0.07	-25
Au	C	**15**	**-0.002**	-0.03	-19
Cu	C	**10**	**-0.002**	0.02	-11
Pt	C	-20	0.002	0.00	**3**
Pd	C	-10	0.001	-0.01	-11
Ni	C	-15	0.003	-0.02	-11

Figure S11. Change in adsorbate charge (Δq) when binding in the presence of a coordinated linker versus when binding on the presence of the bare surface. One plot for each adsorbate, with bar colors indicating the adsorbate according to the bottom color guide.
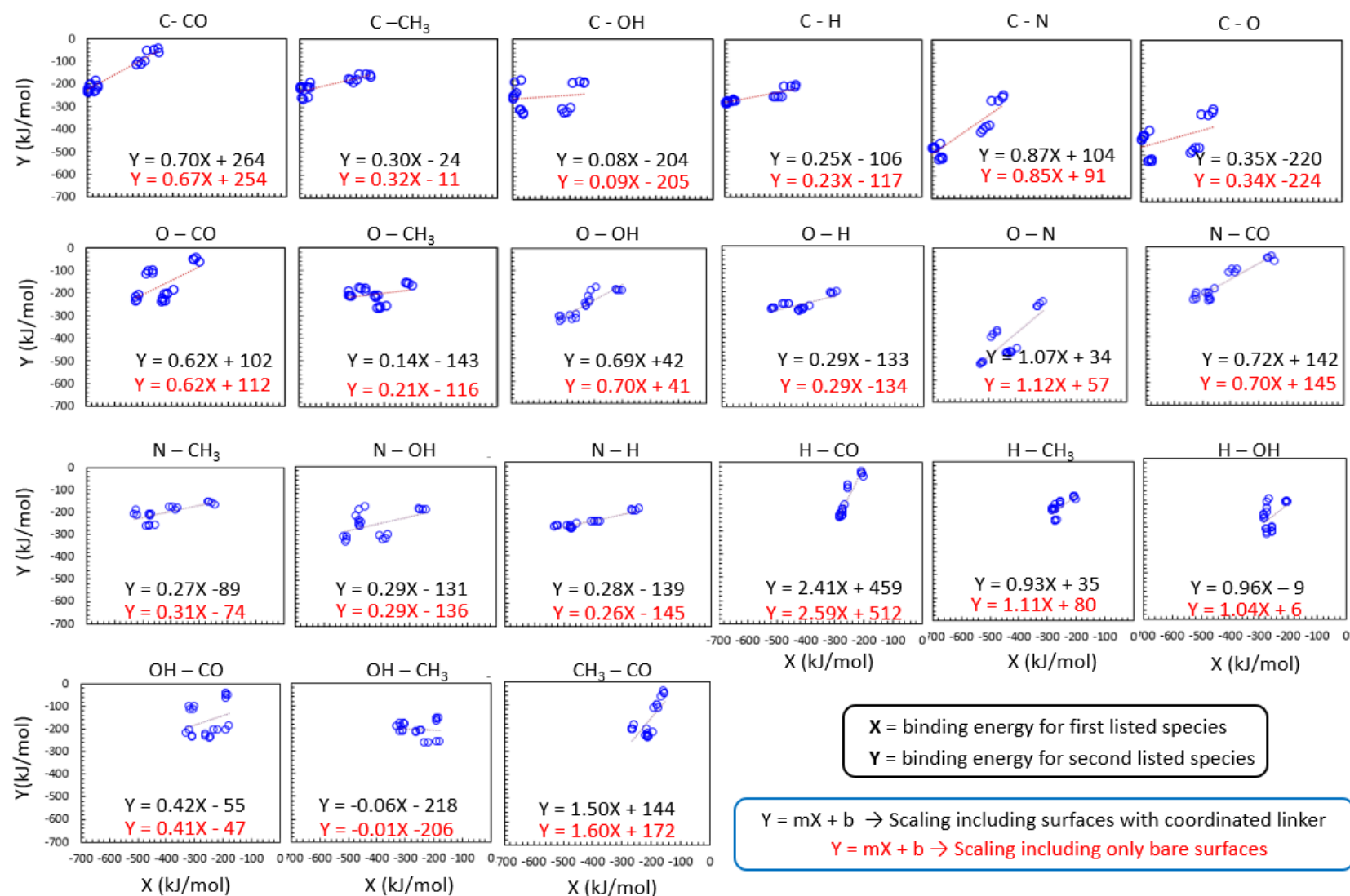
Figure S12. Effect of linker coordination on scaling relationships.

C- CO
$Y = 0.70X + 264$
$Y = 0.67X + 254$

C –CH$_3$
$Y = 0.30X - 24$
$Y = 0.32X - 11$

C - OH
$Y = 0.08X - 204$
$Y = 0.09X - 205$

C - H
$Y = 0.25X - 106$
$Y = 0.23X - 117$

C - N
$Y = 0.87X + 104$
$Y = 0.85X + 91$

C - O
$Y = 0.35X -220$
$Y = 0.34X -224$

O – CO
$Y = 0.62X + 102$
$Y = 0.62X + 112$

O – CH$_3$
$Y = 0.14X - 143$
$Y = 0.21X - 116$

O – OH
$Y = 0.69X +42$
$Y = 0.70X + 41$

O – H
$Y = 0.29X - 133$
$Y = 0.29X -134$

O – N
$Y = 1.07X + 34$
$Y = 1.12X + 57$

N – CO
$Y = 0.72X + 142$
$Y = 0.70X + 145$

N – CH$_3$
$Y = 0.27X -89$
$Y = 0.31X - 74$

N – OH
$Y = 0.29X - 131$
$Y = 0.29X - 136$

N – H
$Y = 0.28X - 139$
$Y = 0.26X - 145$

H – CO
$Y = 2.41X + 459$
$Y = 2.59X + 512$

H – CH$_3$
$Y = 0.93X + 35$
$Y = 1.11X + 80$

H – OH
$Y = 0.96X – 9$
$Y = 1.04X + 6$

OH – CO
$Y = 0.42X - 55$
$Y = 0.41X - 47$

OH – CH$_3$
$Y = -0.06X - 218$
$Y = -0.01X -206$

CH$_3$ – CO
$Y = 1.50X + 144$
$Y = 1.60X + 172$

X = binding energy for first listed species
Y = binding energy for second listed species

$Y = mX + b$ → Scaling including surfaces with coordinated linker
$Y = mX + b$ → Scaling including only bare surfaces
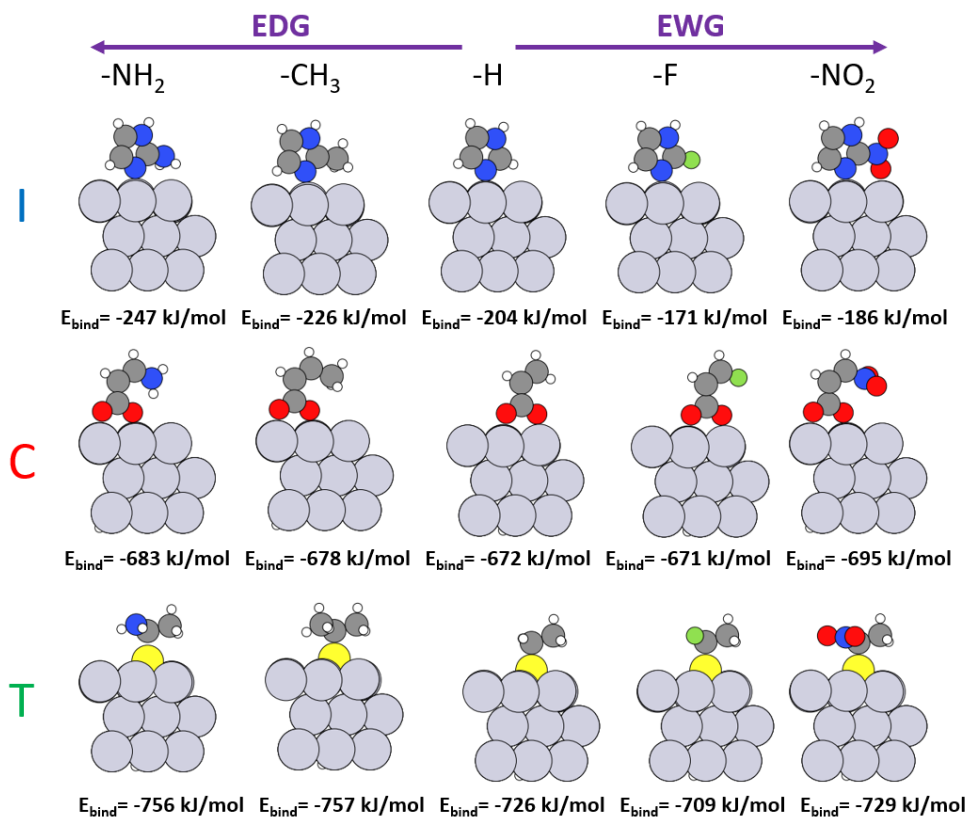
X (kJ/mol)

Y (kJ/mol)

Figure S13. Optimized binding configuration of functionalized linkers on Pt(111) along with binding energy (E_{bind}). I = imidazole, C = carboxylate, T = thiolate.

Table S8. Change in binding energy in kJ/mol for linker binding on Pt(111) due to linker functionalization.

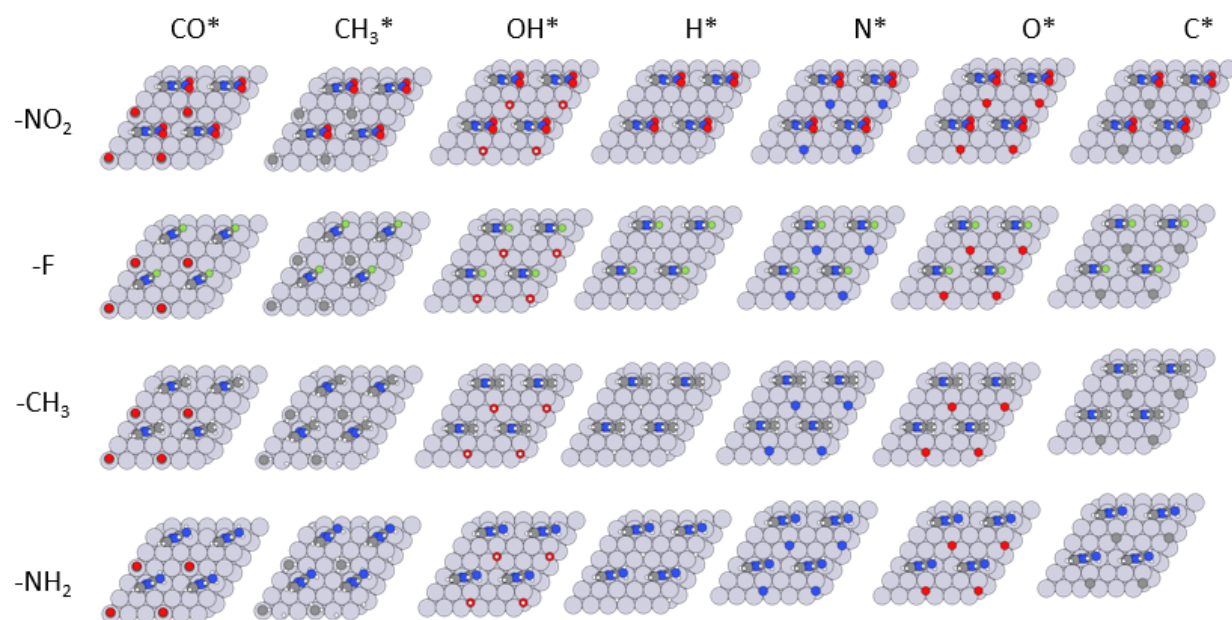| Functionalization	Organic linker		
	I	C	T
-NO$_2$	18	-23	-3
-F	33	1	-17
-CH$_3$	-22	-6	-31
-NH$_2$	-43	-11	-30

Figure S14. Optimized binding configuration of small adsorbates on Pt(111) in the presence of functionalized imidazole linker.
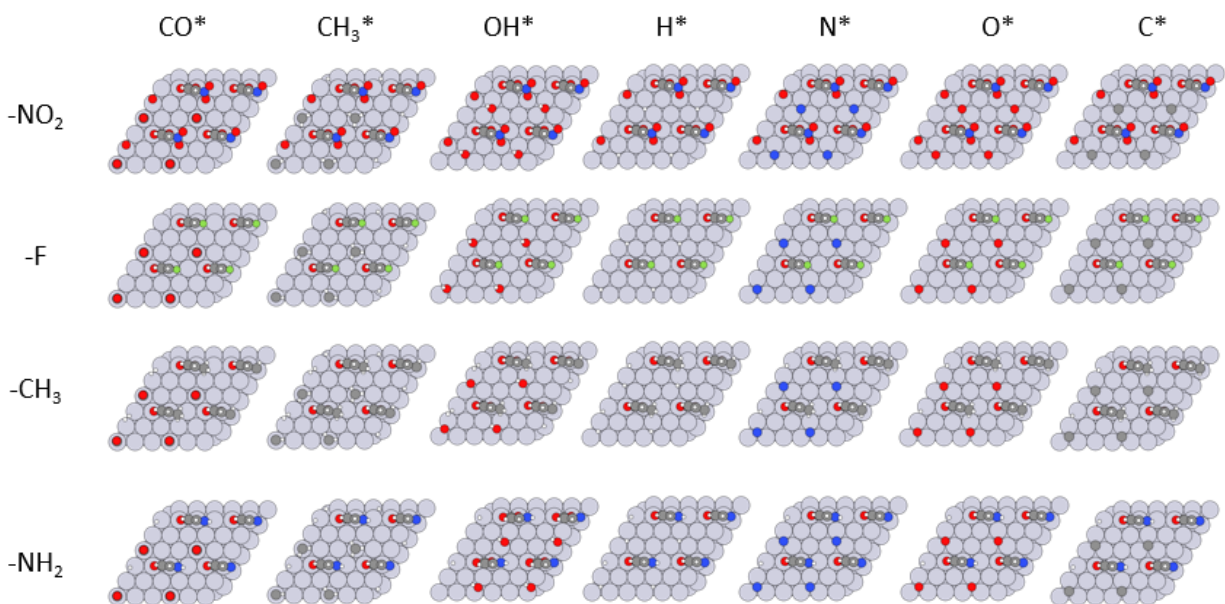

Figure S15. Optimized binding configuration of small adsorbates on Pt(111) in the presence of functionalized carboxylate linker.
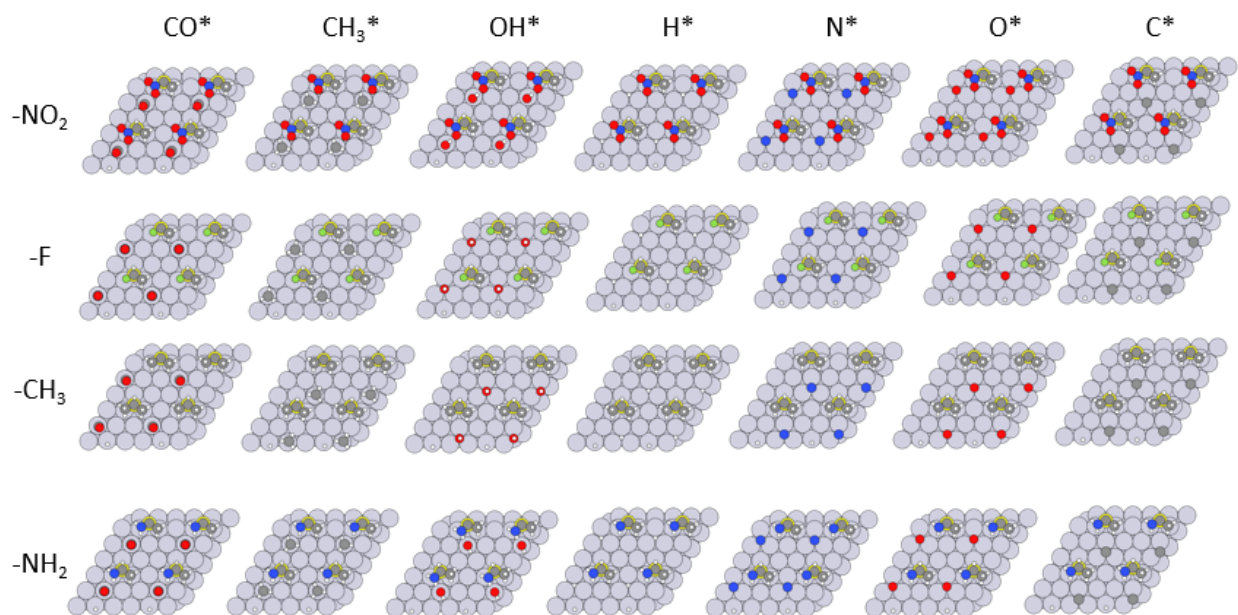
Figure S16. Optimized binding configuration of small adsorbates on Pt(111) in the presence of functionalized thiolate linker.

Table S9. Change in adsorption energy in kJ/mol for adsorbate binding on Pt(111) due to linker functionalization (change calculated relative to binding energy for corresponding unfunctionalized linker case).

	imidazole				carboxylate				thiolate			
	-NO₂	-F	-CH₃	-NH₂	-NO₂	-F	-CH₃	-NH₂	-NO₂	-F	-CH₃	-NH₂
CO*	14	-1	1	2	-4	-2	-2	-2	4	4	5	0
CH3*	19	-1	-1	-3	-4	1	0	2	4	4	10	1
OH*	-10	0	-1	-4	14	-5	-6	-25	-78	-8	2	-99
H*	2	0	0	-1	-1	2	2	1	0	0	0	1
N*	4	-1	-1	0	-6	-3	-4	-3	-5	-5	0	-5
O*	3	-1	-1	0	-6	-6	-7	-6	-11	-11	0	-10
C*	5	-1	-2	-1	-11	-10	-10	-10	0	0	-1	-1

	CO*	CH$_3$*	OH*	H*	N*	O*	C*
PdZn	E_{ads}= -111 kJ/mol	E_{ads}= -162 kJ/mol	E_{ads}= -308 kJ/mol	E_{ads}= -247 kJ/mol	E_{ads}= -355 kJ/mol	E_{ads}= -457 kJ/mol	E_{ads}= -482 kJ/mol
PdAg$_3$	E_{ads}= -160 kJ/mol	E_{ads}= -183 kJ/mol	E_{ads}= -258 kJ/mol	E_{ads}= -257 kJ/mol	E_{ads}= -304 kJ/mol	E_{ads}= -374 kJ/mol	E_{ads}= -499 kJ/mol
PdCu$_3$	E_{ads}= -147 kJ/mol	E_{ads}= -183 kJ/mol	E_{ads}= -316 kJ/mol	E_{ads}= -266 kJ/mol	E_{ads}= -380 kJ/mol	E_{ads}= -451 kJ/mol	E_{ads}= -530kJ/mol
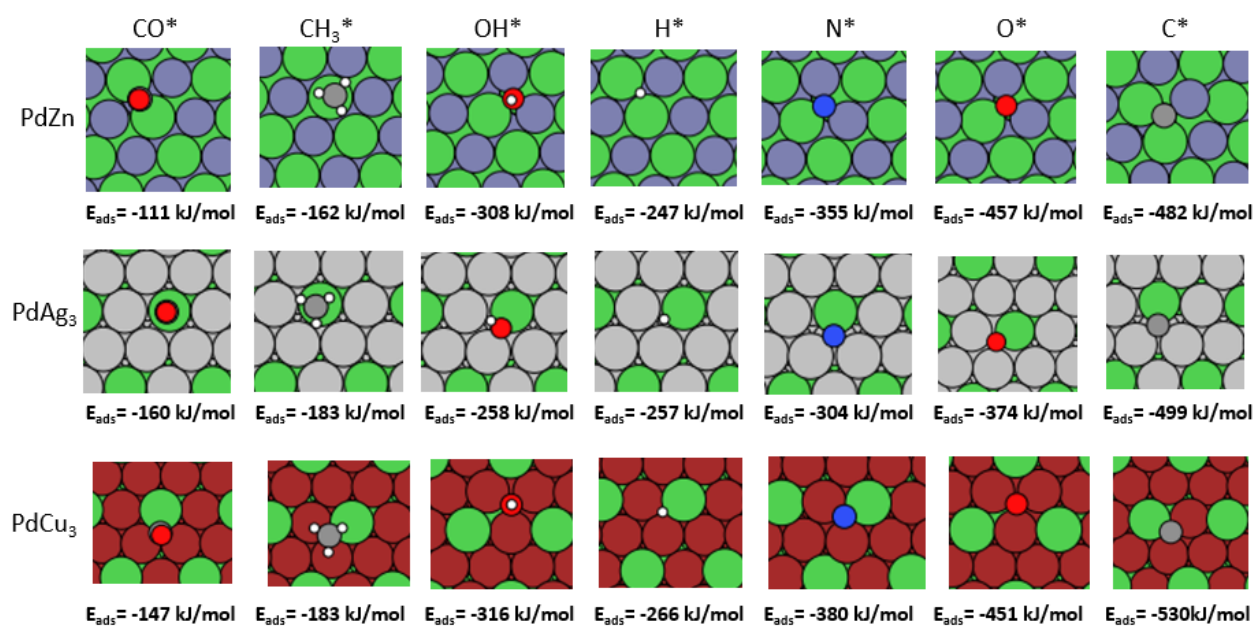
Figure S17. Optimized binding configuration of adsorbates in Pd alloys.

Table S10. Reactions for microkinetic model built in CatMap.

Reaction number	Reaction
1	$C_4H_9OH^* \leftrightarrow C_4H_9OH_{(g)} + *$
2	$O_{2(g)} + * \leftrightarrow O_2^*$
3	$H_2O^* + O_2^* + * \leftrightarrow H_2O\text{--}O_2^* + 2^* \rightarrow 2OH^* + O^*$
4	$C_4H_{10(g)} + * \leftrightarrow C_4H_{10}^*$
5	$2H^* \leftrightarrow H_{2(g)} + 2^*$
6	$C_4H_9^* + O^* \leftrightarrow O\text{--}C_4H_9^* + * \rightarrow C_4H_9O^* + *$
7	$C_4H_9O^* + H^* \leftrightarrow H\text{--}C_4H_9O^* + * \rightarrow C_4H_9OH^* + *$
8	$C_4H_9^* + OH^* \leftrightarrow OHH\text{--}C_4H_8^* + * \rightarrow C_4H_8^* + H_2O^*$
9	$C_4H_8^* \leftrightarrow C_4H_7\text{-}H^*$
10	$C_4H_8O^* \leftrightarrow C_4H_8O_{(g)} + *$
11	$C_4H_7\text{-}H^* \leftrightarrow C_4H_{8(g)} + *$
12	$C_4H_9O^* + OH^* \leftrightarrow OH\text{--}C_4H_9O^* + * \rightarrow C_4H_8O^* + H_2O^*$
13	$C_4H_{10}^* + O^* \leftrightarrow O\text{--}C_4H_{10}^* + * \rightarrow C_4H_9O^* + H^*$
14	$C_4H_9O^* + O^* \leftrightarrow HO\text{--}C_4H_8O^* + * \rightarrow C_4H_8O^* + OH^*$
15	$H_2O^* + O^* \leftrightarrow H_2O\text{--}O^* + * \rightarrow 2OH^*$
16	$C_4H_9O^* + * \leftrightarrow H\text{--}C_4H_8O^* + * \rightarrow C_4H_8O^* + H^*$
17	$O_2^* + * \leftrightarrow O\text{--}O^* + * \rightarrow 2O^*$
18	$H_2O^* \leftrightarrow H_2O_{(g)} + *$
19	$C_4H_{10}^* + O^* \leftrightarrow HOH\text{--}C_4H_8^* + * \rightarrow C_4H_9^* + OH^*$
20	$C_4H_9O^* + OH^* \leftrightarrow O\text{--}C_4H_9OH^* + * \rightarrow C_4H_9OH^* + O^*$
21	$C_4H_9^* + OH^* \leftrightarrow OH\text{--}C_4H_9^* + * \rightarrow C_4H_9OH^* + *$
22	$C_4H_{10}^* + OH^* \leftrightarrow OH\text{--}C_4H_{10}^* + * \rightarrow C_4H_9^* + H_2O^*$
23	$C_4H_9^* + O^* \leftrightarrow OH\text{--}C_4H_8^* + * \rightarrow C_4H_8^* + OH^*$
24	$C_4H_{10}^* + *_{\_} \leftrightarrow H\text{--}C_4H_9^* + * \rightarrow C_4H_9^* + H^*$

Table S11. Formation energies of C* and OH* in kJ/mol.

Metal	Bare		Imidazole		Carboxylate		Thiolate	
	C*	OH*	C*	OH*	C*	OH*	C*	OH*
Zn	373	-6	-	-	-	-	-	-
Ag	500	16	-	-	-	-	-	-
Au	443	111	429	117	449	115	407	113
Cu	375	-19	367	-4	379	-19	392	-2
Pt	187	82	202	112	208	64	228	120
Pd	197	40	197	51	200	42	206	58
PdZn	412	-7	-	-	-	-	-	-
PdAg3	396	42	-	-	-	-	-	-
PdCu3	364	-15	-	-	-	-	-	-
Ni	230	-19	217	-6	234	-22	225	-24

Section S2. Model Training Details

The R package `gbm` was used to build all GBM models. We employed the gradient descent algorithm described by Friedman[3] and implemented in the aforementioned package. Each GBM model was tuned on a hyperparameter grid that included interaction depth (the number of splits performed for each of the individual decision trees), the number of trees (i.e. iterations), shrinkage (or the learning rate), and the number minimum number of training observations in the terminal nodes of the individual tree. The grid search yielded values of 9, 100, 0.2, and 10, for these parameters, respectively. The error for each model corresponding to a point on the hyperparameter grid was estimated using three times repeated 10-fold cross validation with random partitioning. The method outlined in Freidman[3] was used to calculate variable importance using our final GBM model. Given the small amount of data we used for fitting, we did not hold out a final test set to plot for a final validation, but rather plotted the predictions the model made on the hold-out set of each cross-validation fold. With this in mind, and again considering the breadth of our training data, we do not consider our final model to be generally predictive. However, the variable importance metrics derived from training are worthy of scrutiny (similar to how the weights of a linear model are commonly analyzed).

References

1.   T. H. Yu *et al.* Finding Correlations of the Oxygen Reduction Reaction Activity of Transition Metal Catalysts with Parameters Obtained from Quantum Mechanics. *J. Phys. Chem. C* **117,** 26598–26607 (2013).
2.   F. Abild-Pedersen *et al.* Scaling Properties of Adsorption Energies for Hydrogen-Containing Molecules on Transition-Metal Surfaces. *Phys. Rev. Lett.* **99,** 16105 (2007).
3.   J. H. Friedman, Greedy Function Approximation : A Gradient Boosting Machine. *Ann. Stat.* **29,** 1189–1232 (2001).